Supplementary information

Durable VO_2 transition layer and defect inactivation in $BiVO_4$ via spontaneous valence-charge control

Dong Su Kim,[a,1] Kun Woong Lee,[a,1] Ji Hoon Choi,[a] Hak Hyeon Lee,[a] Hee Won Suh[a], Ho Seong Lee[c] and Hyung Koun Cho[a,b,]*

[a] School of Advanced Materials Science and Engineering, Sungkyunkwan University, 2066, Seobu-ro, Jangan-gu, Suwon-si, Gyeonggi-do, 16419, Republic of Korea.

[b] Research Center for Advanced Materials Technology, Sungkyunkwan University (SKKU), 2066 Seobu-ro, Jangan-gu, Suwon, Gyeonggi-do, Republic of Korea.

[c] School of Materials Science and Engineering, Kyungpook National University, 80, Daehak-ro, Buk-gu, Daegu 41566, Republic of Korea.

* Corresponding author.

[1] The authors contributed equally to this work.

Tel.: +82 31 290 7364; Fax: +82 31 290 7410; E-mail: chohk@skku.edu

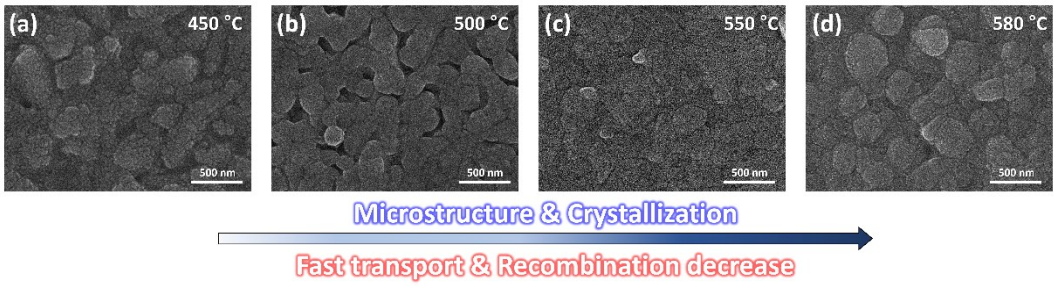

Fig. S1 Comparison of SEM images of the $BiVO_4$ thin film at different annealing temperatures of (a) 450, (b) 500, (c) 550, and (d) 580 °C in the sol-gel process. As the temperature increases, the crystallinity and grain size of the surface increase, and the grain boundary that act as surface defects tends to decrease. Consequently, the mobility of charge carriers increases, and the recombination of charge decreases.

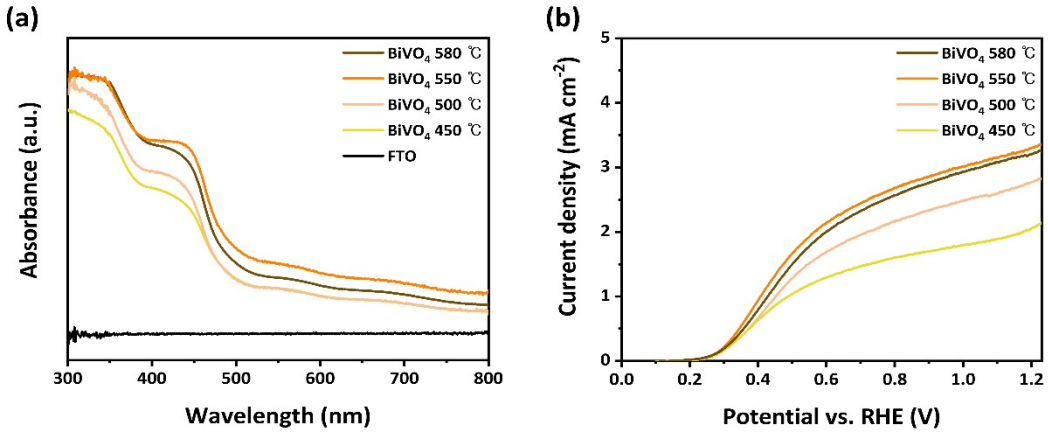

Fig. S2 Evaluations of the $BiVO_4$ thin film at different annealing temperatures (450, 500, 550, and 580 °C). (a) Ultraviolet–visible absorption spectra of $BiVO_4$ and FTO substrates with an integrating sphere from 300 to 800 nm. (b) Linear-sweep voltammetry of $BiVO_4$ photoanodes in 1.0 M PB electrolyte with 0.1M Na_2SO_3 as hole scavenger under AM 1.5 G illumination (100 mW cm^{-2}) with a scan rate of 10 mV s^{-1}.

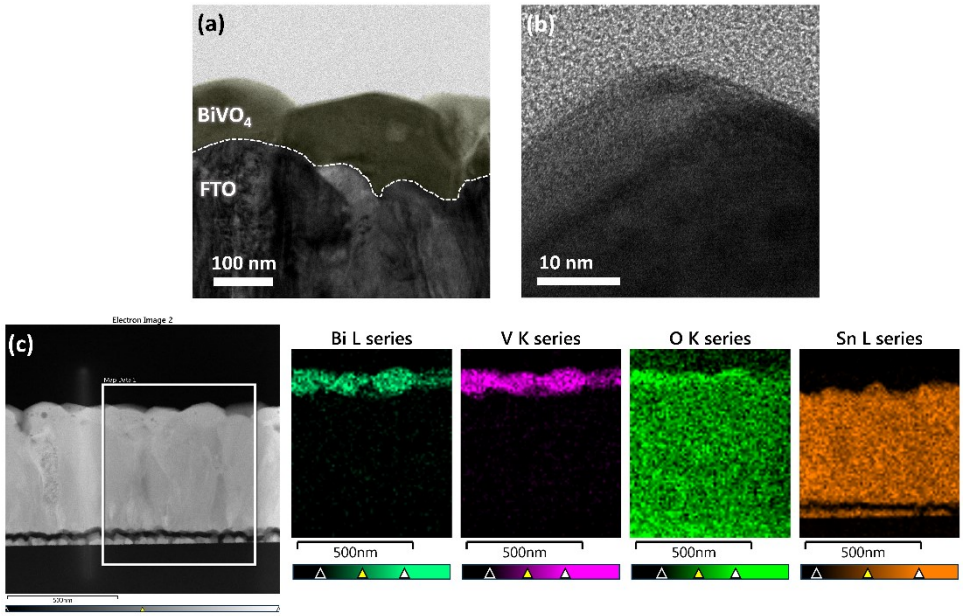

Fig. S3 TEM images of pristine $BiVO_4$ formed through the optimal sol-gel process with an accelerating voltage of 200 KeV. (a) Cross-sectional image of $BiVO_4$ in the form of thin film over 100 nm on the FTO Substrate. (b) High-resolution (HR)TEM image of the $BiVO_4$. (c) STEM-EDS elemental mappings of Bi, V, O, and Sn in the $BiVO_4$ thin film.

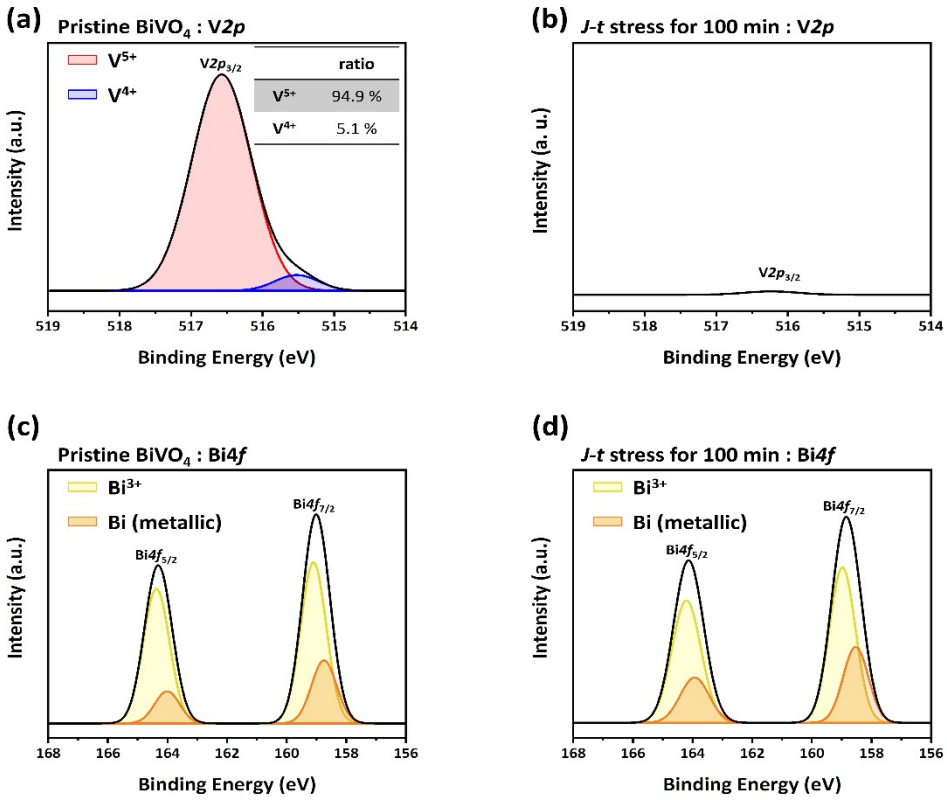

Fig. S4 Fitted XPS spectra of V*2p* and Bi*4f* of pristine $BiVO_4$ and $BiVO_4$ after *J-t* stress for 100 min in the PB electrolyte. (a) is V*2p* of pristine $BiVO_4$, (b) is V*2p* of $BiVO_4$ after *J-t* stress, (c) is Bi*4f* of pristine $BiVO_4$, and (d) is Bi*4f* of $BiVO_4$ after *J-t* stress. In (a), the red area means V^{5+} and the blue area means V^{4+} fitting area. In (b), which was measured in $PEC_{(aq)}$, photo-corrosion occurred because of the long measurement time, and therefore, V*2p* could not be confirmed in XPS spectra. In (c), the yellow area means Bi^{3+} and the orange area means Bi^0 (metallic) fitting area in XPS spectra.

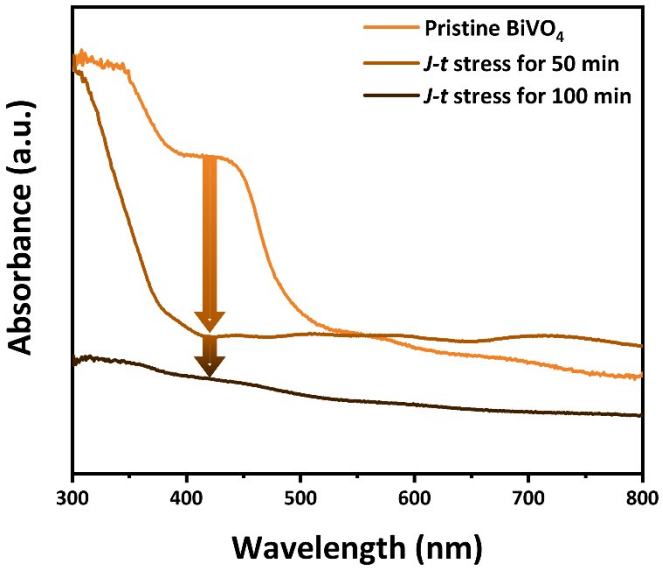

Fig. S5 Ultraviolet-visible absorption spectra of pristine $BiVO_4$ and $BiVO_4$ after *J-t* stress at 1.23 V_{RHE} for 50 and 100 min. The spectra after stress are affected by the bulk as well as the surface properties through photo-corrosion by external applied bias and illumination, and thus, show differences in optical properties.

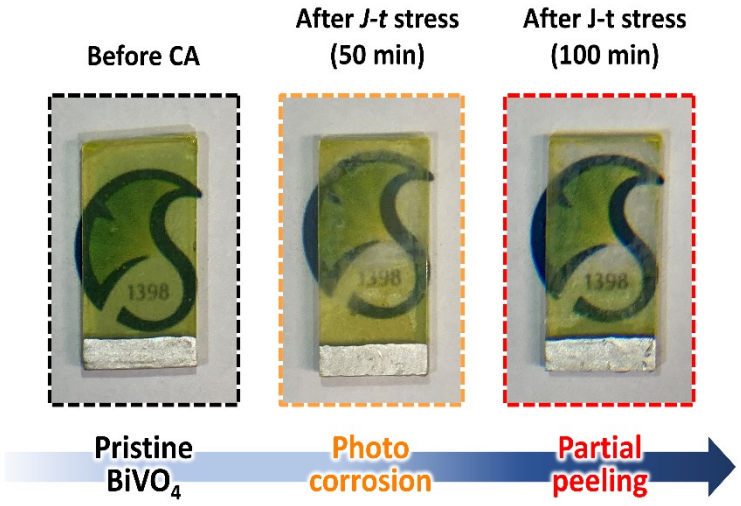

Fig. S6 Optical images of $BiVO_4$ before (black) and after *J-t* stress (CA: chronoamperometry) at 1.23 V_{RHE} for 50 and 100 min. As *J-t* was measured, photo-corrosion occurred on the film surface exposed to light (0.8 × 0.8 cm^2) (orange) and partial peeling occurred intensively in the region where photo-corrosion has progressed (red), according to the photo-corrosion process in Figure 1e. $BiVO_4$ partially peeled by photo-corrosion loses its photo-absorber function.

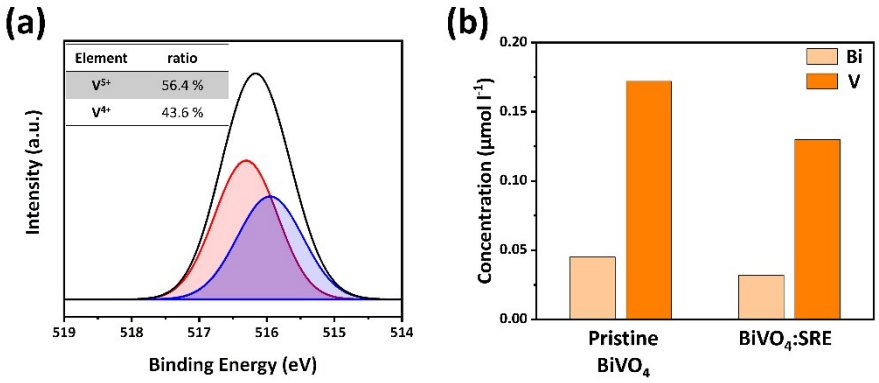

Fig. S7 (a) Fitted XPS spectra of V*2p* $BiVO_4$ after *J-t* stress in $SRE_{(aq)}$. The ratio of V^{5+} and V^{4+} is shown in the inset table. (b) ICP-OES data showing the ion concentration of Bi and V in pristine $BiVO_4$ and $BiVO_4$ after *J-t* stress in $SRE_{(aq)}$.

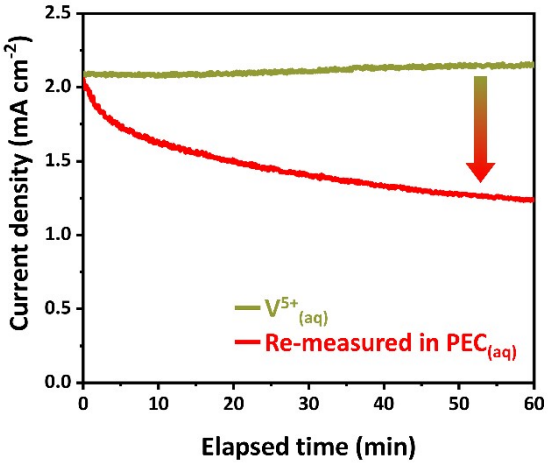

Fig. S8 CA of $BiVO_4$ measured for 5000 s in PEC electrolyte saturated with V^{5+} (green) and re-measured in normal PEC electrolyte (red) under AM 1.5 G illumination (100 mW cm^{-2}) with a scan rate of 10 mV s^{-1}.

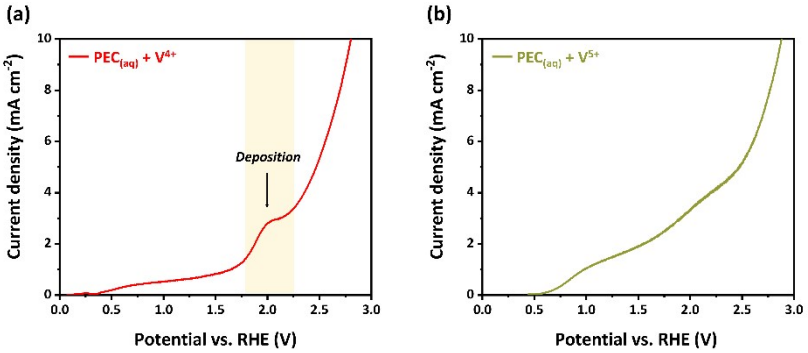

Fig. S9 (a) LSV of $BiVO_4$ in electrolyte saturated with V^{4+} (red line) and (b) LSV plot of $BiVO_4$ in electrolyte saturated with V^{5+} (green line) under AM 1.5 G illumination (100 mW cm^{-2}) with a scan rate of 10 mV s^{-1}. The electrolyte saturated with V^{4+} is prepared by adding 0.1M $VOSO_4$ directly to the PB electrolyte.

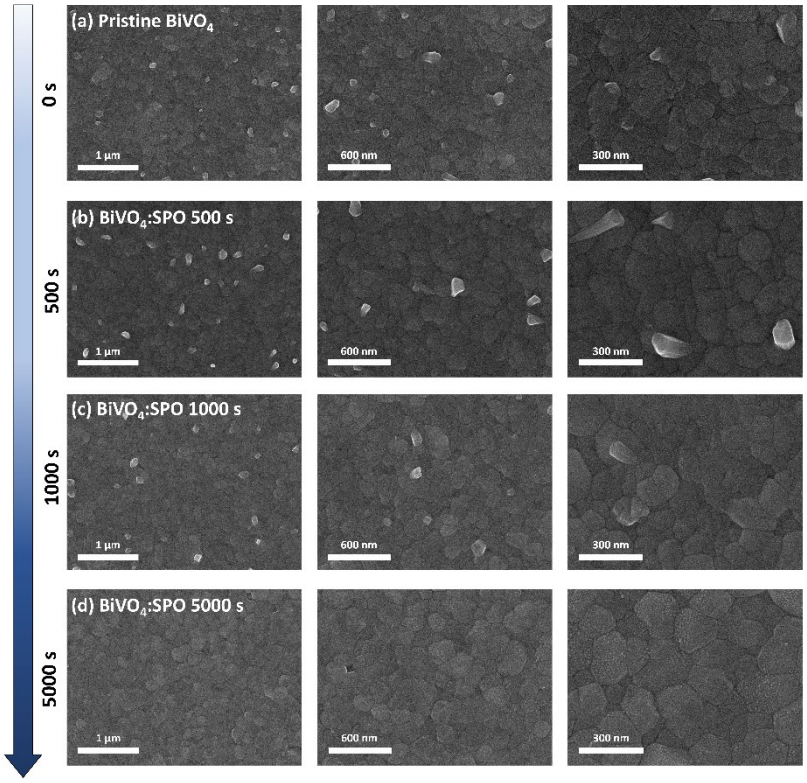

Fig. S10 SEM images of the surface-morphology change of $BiVO_4$ depending on SPO process time: (a) before SPO, and after (b) 500, (c) 1000, and (d) 5000 s.

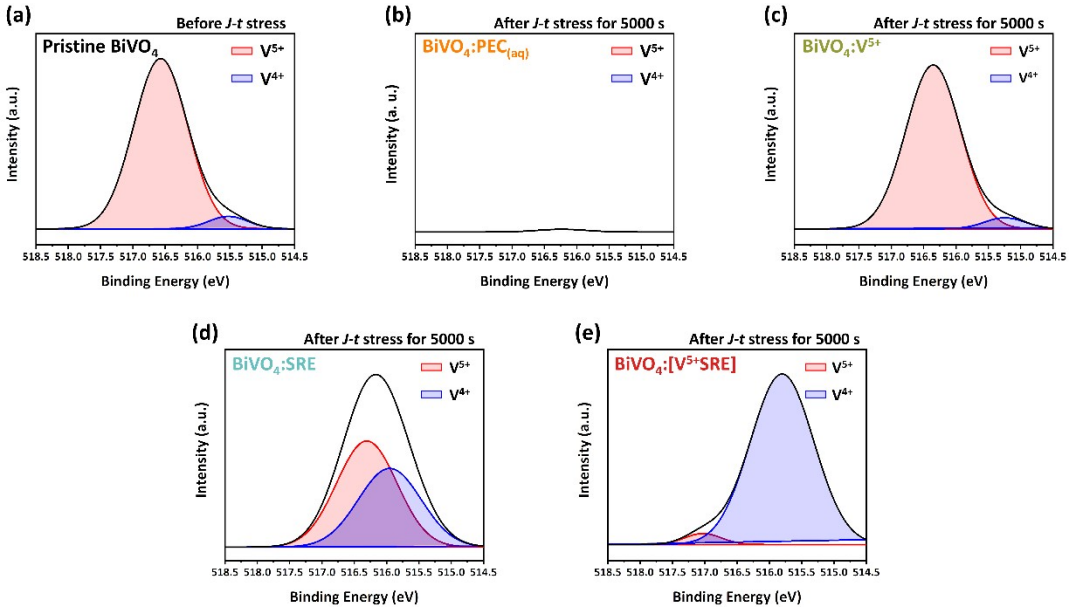

Fig. S11 Fitted XPS spectra of V$2p_{3/2}$ of pristine $BiVO_4$ and $BiVO_4$ after *J-t* stress for 5000 s in different electrolytes: (a) pristine; (b) in $PEC_{(aq)}$; (c) in $V^{5+}{}_{(aq)}$; (d) in $SRE_{(aq)}$; (e) in $V^{5+}SRE_{(aq)}$. The red and blue areas are V^{5+} and V^{4+} fitting areas, respectively.

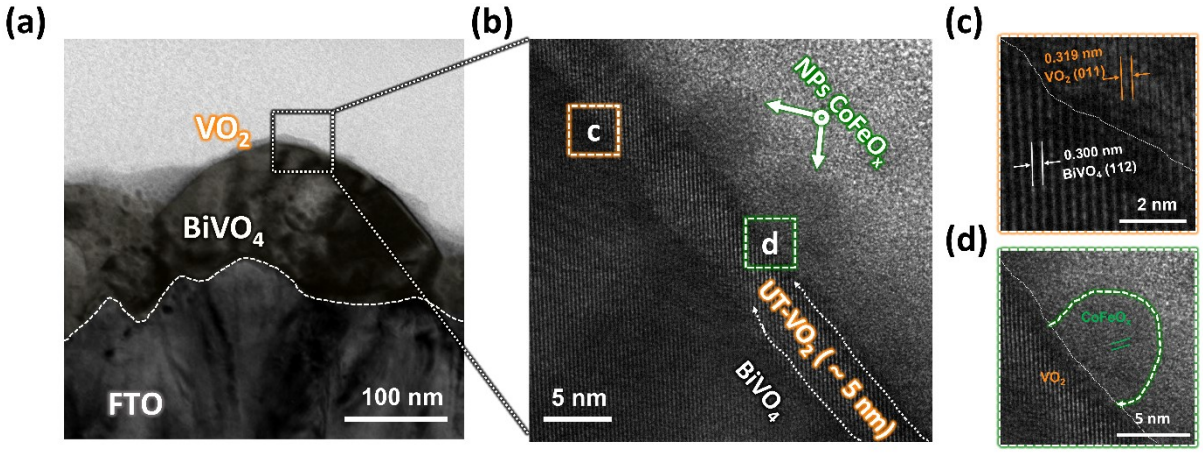

Fig. S12 HR-TEM images of the $BiVO_4/VO_2/CoFeO_x$ photoanode obtained at an accelerating voltage of 200 keV. (a) Cross-sectional image of the photoanode on the FTO Substrate. (b), (c), and (d) Enlarged HRTEM images of the photoanode.

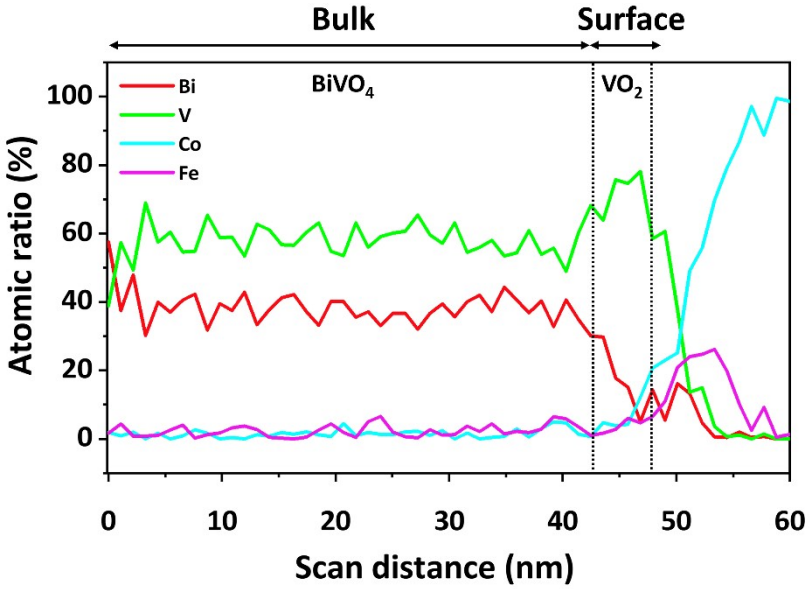

Fig. S13 EDX line profiling of $BiVO_4/VO_2/CoFeO_x$ photoanode.

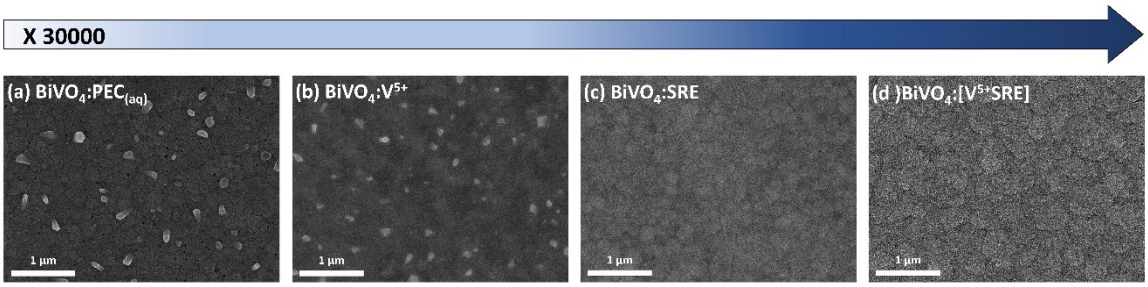

Fig. S14 SEM images of the surface morphology change of $BiVO_4$ after *J-t* stress in different electrolytes for 5000 s. (a) in $PEC_{(aq)}$, (b) in $V^{5+}{}_{(aq)}$, (c) in $SRE_{(aq)}$, and (d) is in $V^{5+}SRE_{(aq)}$.

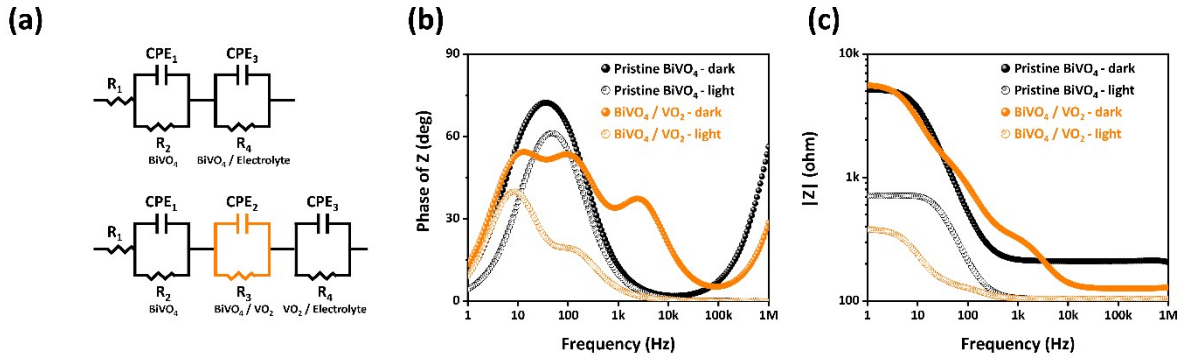

Fig. S15 (a) Equivalent circuit for $BiVO_4$ (top) and $BiVO_4/VO_2$ (bottom) photoanodes. (b) Bode phase plot of the photoanodes. (c) Bode plots of phase and magnitude of Z against frequency in the dark and illuminated states.

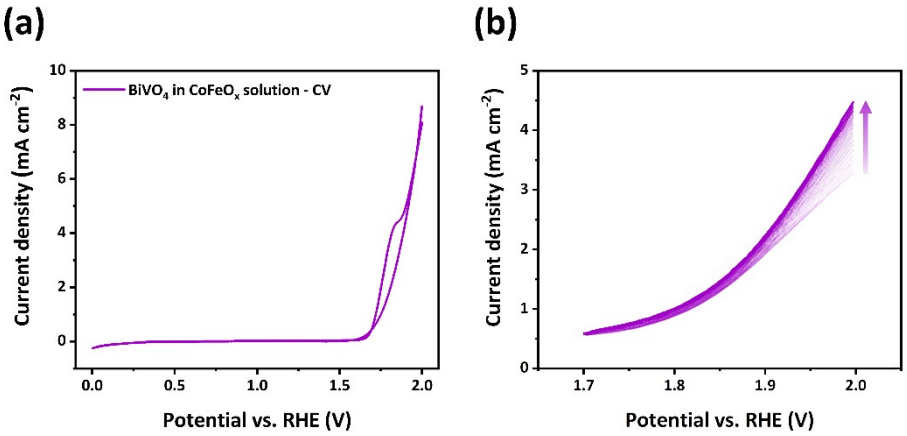

Fig. S16 (a) Cyclic voltammetry of $BiVO_4$ from 0 to 2.0 V_{RHE}. (b) Consecutive-linear-sweep voltammetry (30 cycles) plot of $BiVO_4$ at from 1.7 to 2.0 V_{RHE} in the $CoFeO_x$ deposition solution under AM 1.5 G illumination (100 mW cm^{-2}) with a scan rate of 10 mV s^{-1}.

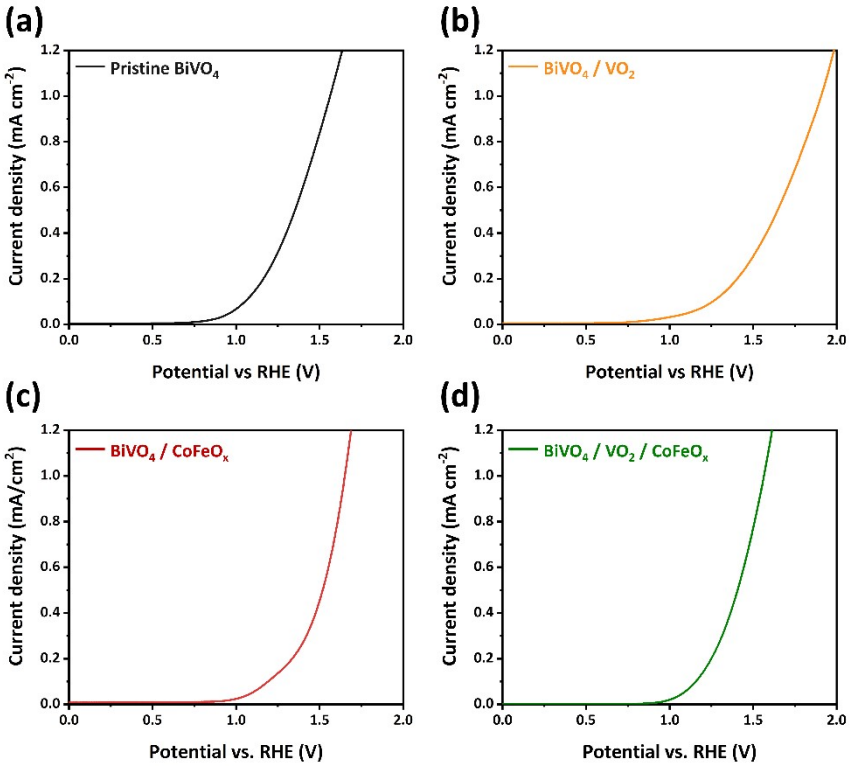

Fig. S17 LSV of photoanodes from 0 to 2.0 V_{RHE} in the PB electrolyte in a dark state with a scan rate of 10 mV s^{-1}: (a) pristine $BiVO_4$; (b) $BiVO_4/VO_2$; (c) $BiVO_4/CoFeO_x$; (d) $BiVO_4/VO_2/CoFeO_x$ photoanodes.

Table S1 Comparison of V^{4+} and V^{5+} fitting-area ratios and binding energies at V$2p_{3/2}$ peak of X-ray photoelectron spectra of pristine $BiVO_4$ and $BiVO_4$ after *J-t* stress in different electrolytes.

	Pristine $BiVO_4$	**$BiVO_4$: $PEC_{(aq)}$**	**$BiVO_4$:V^{5+}**	**$BiVO_4$:SRE**	**$BiVO_4$: [V^{5+}SRE]**
V^{4+}/V^{5+} area ratio (Center peak position, eV)	0.14 (516.60)	Corrosion (516.35)	0.12 (516.36)	0.77 (516.15)	7.63 (515.81)

Table S2 Comparison of X-ray photoelectron peak intensities of Bi*4f*, V*2p*, and O*1s* in pristine $BiVO_4$ and $BiVO_4$ after *J-t* stress in different electrolytes. In the $PEC_{(aq)}$ condition, the calculated V*2p* value is remarkably low, because of V^{5+} dissolution by photo-corrosion.

	Pristine $BiVO_4$	**$BiVO_4$:$PEC_{(aq)}$**	**$BiVO_4$:V^{5+}**	**$BiVO_4$:SRE**	**$BiVO_4$: [V^{5+}SRE]**
Bi*4f*	15.51	20.41	14.42	16.48	12.92
V*2p*	11.57	0.59	8.25	10.73	13.24
O*1s*	72.92	79.00	77.33	72.79	73.84

Table S3 Comparison of EDX composition results in the bulk regions of pristine $BiVO_4$ and $BiVO_4$ after *J-t* stress in different electrolytes. The decrease of Bi*4f* and increase of V*2p* through surface photoelectrochemical oxidation resulted in a 1:1 ratio of Bi and V, indicating modification of unstable $BiVO_4$.

	Pristine $BiVO_4$	**$BiVO_4$:$PEC_{(aq)}$**	**$BiVO_4$:V^{5+}**	**$BiVO_4$:SRE**	**$BiVO_4$: [V^{5+}SRE]**
Bi*4f*	5.41	5.57	5.48	5.42	5.50
V*2p*	4.02	3.46	4.14	4.62	5.89
O*1s*	70.37	70.70	70.05	69.73	68.51
Sn	20.20	20.27	20.33	20.23	20.10

Table S4 Performance comparison. Comparison of photoelectrochemical performances of photoanodes composed of protection layers and oxygen-evolution catalysts based on pristine $BiVO_4$. $J_{ph}^{1)}$ is the photocurrent density (mA cm^{-2}) of a single layer of pristine $BiVO_4$ at 1.23 V_{RHE}; $J_{ph}^{2)}$ is the photocurrent density (mA cm^{-2}) of $BiVO_4$ having oxygen evolution catalysts, V_{onset} (V_{RHE}) denotes the onset potential.

Structure	Method	$J_{ph}^{1)}$	$J_{ph}^{2)}$	Stability	V_{onset}	ABPE (%)	Electrolyte	Ref.
$BiVO_4/VO_2/CoFeO_x$	Sol-gel/SPO/PED	1.3	6.2 ↑↑	100 h (1.23 V)	0.25	2.40 ↑↑	PB	This work
$Mo:BiVO_4$/Co-Ci	Sol-gel/PED	1.2	4.7	1 h (1.0 V)	0.30	-	Bicarbonate	[1]
$N_2:BiVO_4$/FeOOH/NiOOH	ED/ED	1.4	4.8	500 h (0.6 V)	0.22	2.20 ↑	KPi	[2]
$Mo:BiVO_4$/Co-Pi	Dip coating/PED	1.9	4.6	-	0.48	1.09	KPi	[3]
[001] $BiVO_4$/Co-Pi	Laser ablation/ED	3.9 ↑↑	6.1 ↑	6 h (0.6 V)	0.15	-	KPi	[4]
$Mo:BiVO_4$/NiOOH/FeOOH	MOD/PED	2.0	5.0	8 h (1.15 V)	0.20	2.08	Potassium chloride	[5]
$BiVO_4/Co(Co_3)_xOH_y$	ED/Hydrothermal method	1.9	5.1	20 h (0.6 V)	0.20	1.87	PB	[6]
$BiVO_4/NiFeO_x$	ED/PED	2.9	5.0	10 h (0.6 V)	0.23	2.25	PB	[7]
$BiVO_4$/NiFeOOH/Co-Ci	Dip coating/PED	1.0	4.1	3 h (1.23 V)	0.30	0.95	Na_2SO_4	[8]
$Mo:BiVO_4/RhO_2$	Drop casting/MOD	2.1	2.7	12 h (1.23 V)	0.25	-	Sea water	[9]
$BiVO_4/Al_2O_3$	Drop casting/ALD	0.5	1.0	-	0.30	-	Phosphate buffer	[10]
$BiVO_4/Al_2O_3$	Hydrothermal method/ED	0.4	0.5	7.5 h (1.23V)	0.38	-	Sodium phosphate	[11]
$BiVO_4$/PdO	ED/ED	1.8	4.9 ↑	80 h (0.6 V)	0.20	1.72	PB	[12]
$BiVO_4/NiO_x$	Sol-gel/ED	0.3	1.6	1 h (1.23 V)	0.31	-	Sodium borate	[13]
$BiVO_4/TiO_2$	ED/ALD	0.6	1.1	40^{th} cycles LSV	0.41	-	KPi	[14]
$BiVO_4/R:TiO_2$	ED/ALD	0.8	2.1	6 h (0.9 V)	0.20	-	PB	[15]
$BiVO_4/BiFeO_3$	Hydrothermal method/Sol-gel	0.2	0.6	2 h (0.6 V)	0.40	-	KPi	[16]
$BiVO_4/A:TiO_2$	ED/ALD	1.3	3.0	3h (1.23 V)	0.53	-	Na_2SO_4	[17]
$C:BiVO_4$/CQDs	ED/Hydrothermal method	1.4	4.8	9h (0.6 V)	0.25	1.61	Borate buffer	[18]
$Mo:BiVO_4/Nb:TiO_2/FeNiO_x$	MOD/ALD/ED	1.5	5.6	16 h (1.23 V)	0.51	-	H_3PO_4 + NaOH	[19]
$BiVO_4/ZnFe2O_4/Co^{2+}$	ED/PED/Dip coating	1.0	3.0	1 h (1.23 V)	0.40	-	Potassium hydroxide	[20]

References

1 J. H. Kim, Y. Jo, J. H. Kim, J. W. Jang, H. J. Kang, Y. H. Lee, D. S. Kim, Y. Jun and J. S. Lee, *ACS Nano*, 2015, **9**, 11820–11829.

2 T. W. Kim, Y. Ping, G. A. Galli and K. S. Choi, *Nat. Commun.*, 2015, **6**, 1–10.

3 M. Rohloff, B. Anke, S. Zhang, U. Gernert, C. Scheu, M. Lerch and A. Fischer, *Sustain. Energy Fuels*, 2017, **1**, 1830–1846.

4 H. S. Han, S. Shin, D. H. Kim, I. J. Park, J. S. Kim, P. S. Huang, J. K. Lee, I. S. Cho and X. Zheng, *Energy Environ. Sci.*, 2018, **11**, 1299–1306.

5 J. H. Kim, J. W. Jang, Y. H. Jo, F. F. Abdi, Y. H. Lee, R. Van De Krol and J. S. Lee, *Nat. Commun.*, 2016, **7**, 1–9.

6 R. T. Gao, L. Wu, S. Liu, K. Hu, X. Liu, J. Zhang and L. Wang, *J. Mater. Chem. A*, 2021, **9**, 6298–6305.

7 Y. Kuang, Q. Jia, H. Nishiyama, T. Yamada, A. Kudo and K. Domen, *Adv. Energy Mater.*, 2016, **6**, 2–8.

8 X. Hu, Y. Li, X. Wei, L. Wang, H. She, J. Huang and Q. Wang, *Adv. Powder Mater.*, 2022, **1**, 100024.

9 W. Luo, Z. Yang, Z. Li, J. Zhang, J. Liu, Z. Zhao, Z. Wang, S. Yan, T. Yu and Z. Zou, *Energy Environ. Sci.*, 2011, **4**, 4046–4051.

10 D. G. Wang, Y. Y. Zhang, A. Aldalbahi, L. H. Wang, Q. Li and K. Wang, *Nucl. Sci. Tech.*, 2016, **27**, 1–6.

11 K. R. Tolod, T. Saboo, S. Hernández, H. Guzmán, M. Castellino, R. Irani, P. Bogdanoff, F. F. Abdi, E. A. Quadrelli and N. Russo, *Appl. Catal. A Gen.*, 2020, **605**, 117796.

12 R. T. Gao, X. Liu, X. Zhang and L. Wang, *Nano Energy*, 2021, **89**, 106360.

13 Y. Liang and J. Messinger, *Phys. Chem. Chem. Phys.*, 2014, **16**, 12014–12020.

14 E. Usman, M. Barzgar Vishlaghi, A. Kahraman, N. Solati and S. Kaya, *ACS Appl. Mater. Interfaces*, 2021, **13**, 60602–60611.

15 H. Chen, J. Li, W. Yang, S. E. Balaghi, C. A. Triana, C. K. Mavrokefalos and G. R. Patzke, *ACS Catal.*, 2021, **11**, 7637–7646.

16 J. Xie, C. Guo, P. Yang, X. Wang, D. Liu and C. M. Li, *Nano Energy*, 2017, **31**, 28–36.

17 Y. Zhang, X. Zhang, D. Wang, F. Wan and Y. Liu, *Appl. Surf. Sci.*, 2017, **403**, 389–395.

18 Y. Wang, D. Chen, J. Zhang, M. S. Balogun, P. Wang, Y. Tong and Y. Huang, *Adv. Funct. Mater., 2022, **32**, 2112738*

19 M. Beetz, S. Häringer, P. Elsässer, J. Kampmann, L. Sauerland, F. Wolf, M. Günther, A. Fischer and T. Bein, *Adv. Funct. Mater.*, 2021, **31**, 1–8.

20 T. W. Kim and K. S. Choi, *J. Phys. Chem. Lett.*, 2016, **7**, 447–451.